

Article

# Modelling of Lubricated Electrical Contacts

Robert L. Jackson <sup>1,\*</sup>  and Santosh Angadi <sup>2</sup> <sup>1</sup> Department of Mechanical Engineering, Auburn University, Auburn, AL 36849, USA<sup>2</sup> Department of Mechanical Engineering, Nitte Meenakshi Institute of Technology, Bengaluru 560064, Karnataka, India; santosh.angadi@nmit.ac.in

\* Correspondence: jacksr7@auburn.edu

**Abstract:** Electrical contacts, although critically important for a wide range of applications, are susceptible to degradation due to fretting corrosion, especially when sliding and vibrations occur. To overcome fretting corrosion and sliding wear, lubricants are often used. However, the use of lubricants can cause other detrimental issues. Lubricants usually consist of non-conductive fluids such as hydrocarbons and fluorocarbons. Due to fluid dynamics, when sliding, vibration or other excitation occurs, these fluids can cause prolonged gaps between the conducting metal surfaces. Practically, this has been observed in data centers where vibrations due to technician maintenance or even earthquakes can occur. Depending on the viscosity and roughness of the surfaces, the time it takes these connector surfaces to return to solid conductive contact can be many seconds or longer. This work uses a novel theoretical model of the coupled fluid and solid mechanics between the rough metallic surfaces to evaluate these intermittent breaks in contact due to sliding. The influence of variation in lubricant properties, roughness, contact radius and contact force are considered by the model.

**Keywords:** rough surface contact; elasto-hydrodynamic; electrical contact resistance; mixed lubrication



**Citation:** Jackson, R.L.; Angadi, S. Modelling of Lubricated Electrical Contacts. *Lubricants* **2022**, *10*, 32. <https://doi.org/10.3390/lubricants10030032>

Received: 13 December 2021

Accepted: 17 February 2022

Published: 22 February 2022

**Publisher's Note:** MDPI stays neutral with regard to jurisdictional claims in published maps and institutional affiliations.



**Copyright:** © 2022 by the authors. Licensee MDPI, Basel, Switzerland. This article is an open access article distributed under the terms and conditions of the Creative Commons Attribution (CC BY) license (<https://creativecommons.org/licenses/by/4.0/>).

## 1. Introduction

Lubrication is important in the regions of electrical contacts that are found in electrical components such as circuit breakers, electric switches, switchgear connectors, electrical connectors, automotive connectors, printed circuit board (PCB) electronic connectors, connectors in avionics and micro-electro-mechanical systems (MEMS) [1]. The electrical contacts in most of these examples are subjected to sliding situations. Sliding contact, in general, consists of the relative velocities between the two peripheral or outermost surfaces at their contact point [2].

The three regimes of lubrication are usually classified as hydrodynamic or full film, mixed and boundary lubrication [3]. In full-film lubrication, the thickness of the fluid film between the two surfaces is much greater than the surface roughness. This leads to complete separation between the surfaces without any asperity contact. Thus, the friction and wear are significantly low. Now, coming to the mixed lubrication, which falls in between the hydrodynamic (full film) and boundary lubrication regimes, the asperities on the two surfaces are not completely separated here owing to the insufficient film thickness. Hence, the friction and wear will be more. Upon further decrease in the film thickness, there will be a corresponding increase in friction. As the saturation point is reached, this regime of lubrication is termed as boundary lubrication wherein the asperity contact between the two surfaces is greatly enhanced such that both friction and wear will usually be very high.

The key lubricant properties are viscosity, corrosion, operating temperature, fire resistant, specific gravity, etc. [4]. Moreover, the hydrodynamic lubrication regime is focused upon in this work. A thorough review of the existing literature on the sliding electrical contact including its lubrication, fretting corrosion and contact resistance aspects is

considered next wherein the relevant efforts globally, and in the past, by various researchers are summarized aptly.

One of the earliest works that stressed upon the necessity to provide prime importance towards the research in the field of electrical contacts' lubrication was by Campbell [5]. The author explained the lubrication principles such as hydrodynamic lubrication and boundary lubrication. The type of contacts addressed here were sliding contacts. Moreover, the associated lubricant properties, such as corrosion, viscosity, creep and stability to oxidation were discussed in this work [5]. Continuing further, in 2005, Chudnovsky [6] carried out a thorough review on the research pertaining to the lubrication of electrical contacts. In this work, the importance and use of lubrication at the contact level were emphasized [6].

The role of lubricants in electrical contact situations is explained now in detail. At first, a key benefit of a lubricant in electrical contacts is its ability to reduce their oxidation, which thus facilitates to achieve an increased stable lifetime of the associated components [7,8]. Secondly and most importantly, lubrication not only serves as a protection for the contact surfaces towards corrosion but also helps in the reduction of the adhesive friction, mechanical wear and fretting-based degradation. In this regard, for a given set of environmental conditions and a particular contact material, it is critical to ensure that the lubricant will thus qualify for its use in the intended application or scenario. However, the lubricant selected must not lead to an increase in the electrical contact resistance. This is because the liquid lubricants are, in general, of a non-conductive type. Thus, the occurrence of a lubricant film at the contacting regions leads to an increment in the contact resistance of electrical contacts due to hydrodynamic lift, formation of tribofilm or degradation of the lubricant itself [9].

To address this issue, a recent work [9] considered metallic nanoparticles as lubricants that help in maintaining a stable and decreased contact resistance in addition to lowering wear and friction. However, during sliding the contact resistance temporarily increased and conventional lubricant additives often caused a permanent change in resistance. In an extension to this work, Crilly et al. [10] focused upon the characterization of contact resistance, friction and wear by employing a silver nanolubricant involving dodecane under the conditions of low force applicable in the case of smaller contacts and comparing to a conventional hydrocarbon-based lubricant. Furthermore, in 2019, Cao et al. [11] employed ionic liquids (ILs) as a lubricant for sliding electrical contacts consisting of copper to enhance their lifetime and reliability. The results of this investigation suggested that ILs contribute for reducing the ECR, coefficient of friction and wear volume. Stable ECR is also observed due to this lubricant during usage.

Studies by Ko et al. [12] also revealed that the electrical contact resistance decreases owing to the use of gold nanoparticles as a lubricant in the electrical contacts of the MEMS switches [12]. Likewise, Berman et al. [13] evaluated the effectiveness of applying graphene in the form of a lubricant for sliding electrical contacts. Along with the reduced wear and friction demonstrated by this lubricant, it also aids in lowering the sliding electrical contact resistance that is also stable for dry and humid environmental test conditions involving sliding passes of the order of thousands [13]. Lang et al. [14] also considered graphene as a solid lubricant for sliding electrical contacts. The authors found that the use of graphene yields ultrahigh current stability, ultra-low friction and improved wear resistance. Furthermore, in 2008, Achanta and Drees [15] found that the fretting wear loss can be reduced by implementing di-electric greases as the lubricants in the electrical contacts coated with gold [15]. Kaushik et al. [16] also found that PFPE lubricants could form an insulating layer detrimental to gold electrical contact, but that PAO was not observed to do this. In a continuation of this work, it was mentioned that hydrodynamic lubrication (studied in this work) also caused PFPE to insulate the electrical contacts [17]. Swingler also showed that lubricants are very effective in reducing fretting wear in automotive connectors and removing wear debris, but can degrade in powered contacts [18].

Graton et al. [19] investigated the influence of lubrication consisting of conductive grease on the electrical endurance (DC and RF) of electrical contacts plated with gold material. Fretting wear tests were performed on these contacts in both lubricated and dry conditions. The results indicated that the coefficient of friction (COF) ( $\mu$ ) lowered significantly due to grease lubrication. Thus, the oxidation and wear of the contact surfaces were prevented, thereby leading to an enhancement of their electrical lifetime [19]. Recently, in 2021, the same effect of reduced COF was also noticed by Fu et al. [20]. To extend this discussion related to greases in electrical contacts, Noël et al. [21] conducted laboratory fretting tests on the grease lubricated tinned connector contacts. For specific experimental test conditions, a variety of commercial greases were considered, and their behavior was compared. The results of room temperature tests showed a minimal effect on the electrical behavior of these contacts. However, upon prolonged heat treatment at 150 °C, a few cases exhibited a very large rise in the contact resistance. The authors suggested that the usage of grease consisting of thickener and base oil has a negative influence on the electrical contact application [21]. In another work by Larsson et al. [22], higher fretting amplitudes of displacement yielded significant outcomes for the electrical contacts lubricated with grease. These include reduced COF, smooth surfaces and very high contact resistance values [22], which could be detrimental in some electrical contacts.

Amada et al. [23] studied the sliding electrical contacts in the lubricated copper ring-carbon brush systems through experimental test equipment. The results show that the lubricants will affect the contact resistance of these contact systems [23]. Furthermore, in 2015, Sawa et al. [8] investigated the lubricated contact systems made up of AgPd brushes and Au-plated slip-rings in terms of the contact voltage fluctuation. The authors indicated that this fluctuation is due to the lubricant film [8]. In a closely related earlier work by Sawa et al. [7] on these electrical contact configurations, a key finding is that the presence of lubricant in the ring will increase its contact resistance [7].

As will be discussed, the current work also considers the elastic deformation of the surfaces due to hydrodynamic lifting pressure and rough surface contact. This work could therefore, be considered an elasto-hydrodynamic lubrication problem [24], but while considering roughness and electrical contact. Although this mechanism of lubrication and the resulting film thickness has been experimentally confirmed for both relatively smooth [25] and rough surfaces [26], it has not been investigated extensively for electrical contacts.

The originality of this work is that the sporadic electrical contact gaps or breaks in rough contact surfaces have been evaluated through the development of a new theoretical model involving the mechanical and fluid coupled fields. In addition, this model encompasses the effect of changes in contact resistance and lubricant as well as material properties. The above literature review indicates that such a model is non-existent to date. references.

## 2. Numerical Methods

Although it is known that lubricated electrical contacts can have intermittent increases in the contact resistance when vibrations or sliding motions occur, little work has been performed to theoretically investigate this phenomena. Therefore, a numerical simulation of a lubricated electrical contact system is created to provide a predictive model, and an improved understanding of lubricated electrical contact behavior. The numerical model is capable of considering new design variations to avoid connector distress and disconnects, such as variations in materials, roughness, lubricants and geometries. A coupled set of mechanical solid and fluid models are solved simultaneously using an iterative algorithm. A quasi-steady state solution is produced after the numerical algorithm converges and the error is below a specified criteria. The interfacial contact forces and fluid pressure between the components change as the displacement between the surfaces is adjusted until the model converges to a solution.

Below we outline the numerical formulation and theoretical sub-models used in the electrical contact simulation, and then the results are discussed. The physical sub-models used to consider the mechanisms include elasto-plastic asperity contact, mixed and full-film

lubrication, elastic surface deformation and a force balance. The force balance couples together all the considered mechanisms through the fluid and solid contact pressures. This is shown through a flowchart depicting the sequence of calculations that is iterated until the external force balances with the forces from the fluid and solid contact (see Figure 1). The coupled sub-models produce a set of nonlinear equations which are solved numerically. The following sections detail the individual sub-models and the assembled numerical algorithm.

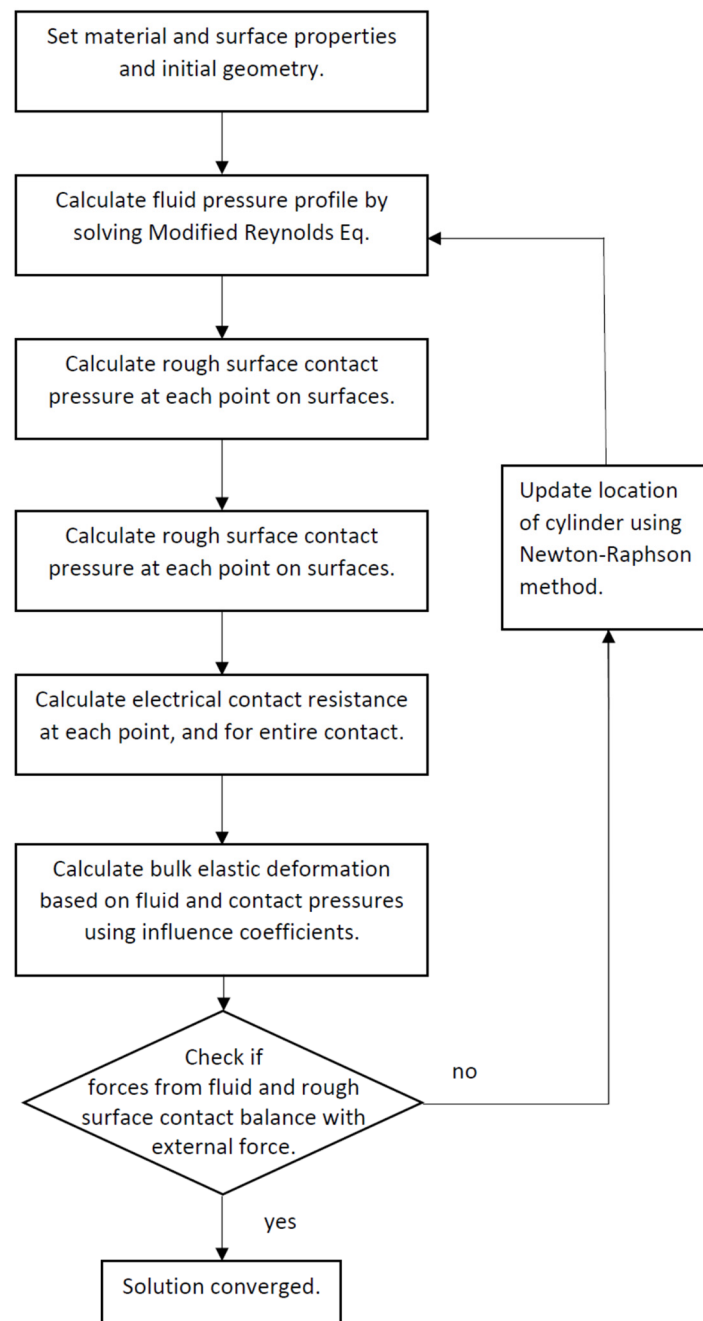


**Figure 1.** Flowchart depicting the sequence of the numerical model.

### 2.1. Assumptions

The numerical simulation makes several assumptions which may result in differences between the results of the numerical and experimental observations. The major assumptions of the model are:

- In the absence of accurate wear and corrosion prediction techniques for lubricated electrical contact conditions, wear and corrosion of the surfaces are not included. The effects of lubricant chemistry at the interfaces, such as tribofilm formation, are not directly considered. In other words, the surface properties, resistivity and roughness topography remain unchanged throughout the simulation, although deflections are considered at the asperity scale and large macro-scales.
- The current quasi-static model neglects time dependent effects such as vibrations and squeeze film effects, but as noted in previous work, this could be important [27].
- Thermal effects, such as heat generation due to Joule heating and friction are ignored, along with temperature dependent properties.

Figure 2 depicts the simple electrical connector system. Note that the connector is simply modeled as a cylindrical surface here, but more complicated geometries could be considered by the model in the future, such as spring geometries and thin layers, which are often used in connectors [28]. Both the cylinder and block will either be in contact, have fluid pressures separating them, or have a combination of both. The vertical position of the cylinder is raised or lowered based on the net forces determined by the physical mechanism sub-models outlined in the following sections.

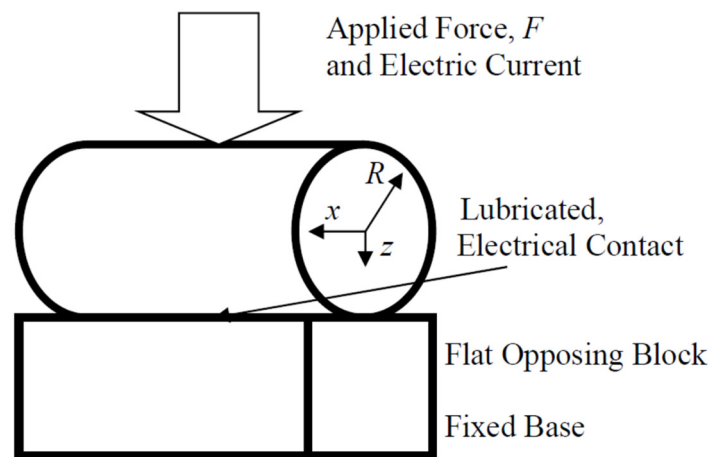


Figure 2. Schematic of the considered electrical contact system.

## 2.2. Hydrodynamic and Mixed Lubrication

In regions of thin films or contact, the roughness of the surfaces influences the fluid flow. This regime of lubrication is known as mixed lubrication. In mixed lubrication, the roughness features, or peaks, act as obstructions to the flow of fluid between the surfaces. Patir and Cheng's [29,30] flow factor method is employed to account for this and results in a modified form of the Reynolds equation:

$$\frac{\partial}{\partial x} \left( \phi_x \frac{h^3}{12\mu} \frac{\partial p}{\partial x} \right) + \frac{\partial}{\partial y} \left( \phi_y \frac{h^3}{12\mu} \frac{\partial p}{\partial y} \right) = \frac{U_1 + U_2}{2} \frac{\partial h}{\partial x} \quad (1)$$

where  $\phi_x$  and  $\phi_y$  are mathematical flow factors that describe the obstruction of the fluid flow from the surface roughness. Patir and Cheng provide flow factor equations which depend on the film thickness, surface roughness and asperity orientation (longitudinal or lateral). The roughness is assumed to be isotropic here and thus the flow factors are independent of the direction of flow. The isotropic flow factor equations given by Patir and Cheng are:

$$\phi_x = \phi_y = 1 - 0.90e^{-0.56(h/\sigma)} \quad (2)$$

where when the film thickness is much larger than the roughness ( $h/\sigma > 6$ ), the flow factors lose influence and the lubrication model automatically reverts to the conventional Reynolds equation. For instance, as  $h/\sigma$  increases  $\phi_x$  and  $\phi_y$  approach the value of one.

The modified Reynolds equation (Equation (1)) when solved produces a prediction of the fluid pressure between the surfaces. The centered finite difference method (FDM) is used to numerically solve Equation (1). Another numerical method that is often used to solve the Reynolds equation is the finite element method (FEM). FEM and FDM can produce very similar results by using different numerical schemes. FDM is a widely used method for solving Reynolds equation problems [31–33]. However, FDM is better for thin films that can be approximately by a two-dimensional laminar flow analysis. FEM might be better suited for more complex geometries [34]. Therefore, FDM is used here.

At each node, a corresponding film thickness,  $h$ , is calculated based on the location of the cylinder,  $z$ , and the surface deformation,  $\delta$ . This is given by

$$h = h_o + z + d \quad (3)$$

at each point on the surface where  $h_o$  is the initial film thickness that includes the undeformed geometry of the cylinder with radius,  $R$ , or

$$h_o = R - \sqrt{R^2 - x^2} \quad (4)$$

Moreover,  $z$  is the vertical location of the cylinder and is increased or decreased by the numerical algorithm as described later. Finally,  $\delta$  is the macro-scale elastic deflection of the surfaces. The predicted fluid and contact pressures at each node on the surface are inputted into an influence coefficient matrix to predict this deformation. The influence coefficient method is based on the numerical methodology outlined in [35–38]. Note that other works on electrical contacts used FEM to consider macro-scale deformation, but they did not consider the inclusion of a lubricant in the contact [39–45]. The influence coefficient is more computationally efficient than FEM and since the analysis is iterative while considering the coupled solid and liquid models, this is important to make a calculation in a reasonable amount of time without sacrificing much accuracy.

At the edge of the cylinder and the inlet and outlet of lubrication, the boundary condition  $p = 0$  is assumed. The Reynolds boundary condition is implemented to consider cavitation in the fluid, i.e., when the pressure is negative it is set to zero. The code iteratively solves the Reynolds equation using the Gauss–Seidel method. Under-relaxation is used to enhance numerical convergence. At each node, the modified Reynolds equation is solved to give the fluid pressure,  $p$ .

The numerical algorithm requires a force balance, and so the net force from the fluid pressure needs to be calculated. Then, the pressure over the connector surface area is numerically integrated to calculate the total fluid force as

$$F_{fluid} = \int_A p dA \quad (5)$$

### 2.3. Elastic-Plastic Rough Surface Contact

The statistical elastic-plastic asperity contact model derived in [46] is employed to consider solid contact of the small scale peaks on the surfaces. The statistical model is used rather than a deterministic finite element model due to the computational efficiency. It is difficult to include the necessary mesh density required to deterministically model rough surface contact effectively, especially when plasticity is included [47]. Using finite elements to predict the elastic perfectly-plastic spherical contact, the following equations were fit to the results (not that Equation (6) is for elastic contact and Equation (7) is for elastic-plastic contact):

For  $0 \leq \omega^* \leq \omega_t^*$

$$\frac{\bar{P}_F}{\bar{P}_c} = \left( \frac{\omega}{\omega_c} \right)^{3/2} \quad (6)$$

For  $\omega_t^* \leq \omega^*$

$$\frac{\bar{P}_F}{\bar{P}_c} = \left[ \exp\left(-\frac{1}{4}\left(\frac{\omega}{\omega_c}\right)^{\frac{5}{12}}\right) \right] \left(\frac{\omega}{\omega_c}\right)^{3/2} + \frac{4H_G}{CS_y} \left[ 1 - \exp\left(-\frac{1}{25}\left(\frac{\omega}{\omega_c}\right)^{\frac{5}{9}}\right) \right] \frac{\omega}{\omega_c} \quad (7)$$

where from [48]

$$\frac{H_G}{S_y} = 2.84 - 0.92 \left[ 1 - \cos\left(\pi \frac{a}{R}\right) \right] \quad (8)$$

and the critical interference to cause initial yielding  $\omega_c$  is derived independently of the hardness, to be:

$$\omega_c = \left( \frac{\pi \cdot C \cdot S_y}{2E'} \right)^2 R_{peak} \quad (9)$$

where  $R_{peak}$  is the average radius of curvature of the peaks and  $C$  is derived to be

$$C = 1.295 \exp(0.736\nu) \quad (10)$$

This single peak contact model is then incorporated in a statistical framework to expand it to an entire rough surface with peaks at various heights. The heights of the peaks are assumed to follow a Gaussian distribution,  $G(z)$ . These statistical equations are then given as [49]:

$$P(d) = \eta A_n \int_d^{\infty} \bar{P}_F(z-d) G(z) dz \quad (11)$$

where  $\eta$  is the peak areal density. The mean surface separation distance is  $h$ , while the mean distance between the peaks of the surface is  $d$ .  $h$  and  $d$  are related by

$$h = d + y_s \quad (12)$$

$y_s$  is given as [50]

$$y_s = \frac{0.045944}{\eta R_{peak}} \quad (13)$$

These rough surface values ( $\eta$ ,  $R_{peak}$ ,  $\sigma$ ) can be approximated from profilometer measurements using the methods outlined in McCool [51]. The average contact force,  $P$ , is predicted by Equation (11) as a function of surface separation,  $h$ . Therefore, at each node the contact force is predicted between the surfaces of the electrical contact. The contact forces on each node are summed together to give the total solid contact force between the surfaces,  $F_{cont}$ .

It should be noted that there is a concern that with repeated loading of the surfaces, perhaps due to the electrical contact being disconnected and connected again. Based on many papers in the literature most metallic contacts will have significant elastic-plastic deformation. That said, several papers show that under repeated loading, the contact will return to the same contact area if the same load is applied (the process is reversible) [52,53]. Therefore, the permanent deformation is included, although it is not predicted. It should also be noted that the process might not be reversible if sliding or friction occurs [54], which is not the case here but could be in some problems.

#### 2.4. Statistical Electrical Contact Resistance

After the statistical model is solved to predict the contact force between the rough surfaces, it can also be employed to predict the electrical contact resistance between the surfaces. Here, the Holm model for spreading contact resistance is used to predict the

electrical resistance at the contact peaks. The Holm model requires the contact radius,  $a$ , to be predicted and here it is given by [55].

$$a_{ep} = \sqrt{D\omega R_{peak}} \quad (14)$$

For  $0 \leq \omega/\omega_c \leq 1.9$ ,  $D = 1$

For  $\omega \geq 1.9$ ,  $D = \left(\frac{\omega}{1.9\omega_c}\right)^B$

By applying the contact radius, the statistical rough surface contact resistance is obtained as

$$\frac{1}{Er_{ep}} = \eta A_n \int_d^{\infty} \frac{2a_{ep}}{\rho_L} G(z) dz \quad (15)$$

However, the above model assumes that the peaks are electrically isolated. The alleviation factor,  $\Psi$ , is used here to consider that the electrical current bottleneck at the peak contacts will be alleviated as more of the surface comes into contact. Cooper et al. [56] give the alleviation factor as

$$\Psi = \left(1 - \sqrt{A_r/A_n}\right)^{1.5} \quad (16)$$

$$Er = Er_{ep}\Psi \quad (17)$$

### 2.5. Force Balance and Numerical Solution

The force balance of the cylinder is satisfied such that the fluid and solid contact forces balance the applied force. The elasto-plastic asperity contact model calculates the total contact force,  $F_{cont}$ . The modified Reynolds equation (Equation (1)) is solved for the fluid pressures which are integrated to provide the total fluid force,  $F_{fluid}$  using Equation (5). The numerical solution is complete when the forces balance as given by:

$$F = (F_{cont} + F_{fluid}) \quad (18)$$

Both the contact and fluid forces depend on the vertical location of the cylinder relative to the block,  $z$ . Thus, the problem is formulated as a nonlinear set of equations (Equations (1)–(18)) with a single unknown,  $z$ . These equations are dependent on the governing physical equations of rough surface contact, mixed and full-film lubrication, macro-scale elastic deformation and a force balance. The unknown,  $z$ , is therefore solved using an iterative process. The Newton-Raphson method is used to increment  $z$  until the forces balance and equation is satisfied, within a set error criteria.

### 2.6. Mesh Convergence

The same nodal grid is used for both the fluid pressure solution (Equation (1)) and the elastic-plastic rough surface contact. The mesh is refined at several densities to confirm that the mesh is fine enough to provide an accurate solution, thus satisfying mesh convergence. The predictions of contact resistance as a function of applied sliding speed are shown in Figure 3. The total number of nodes of each of the meshes differ by approximately a factor of 2. Based on this, and to use a reasonable amount of time for calculations, a  $51 \times 51$  mesh (2601 nodes) is used. Note that although the finer mesh will still provide a more accurate prediction, the computational time was several days long.

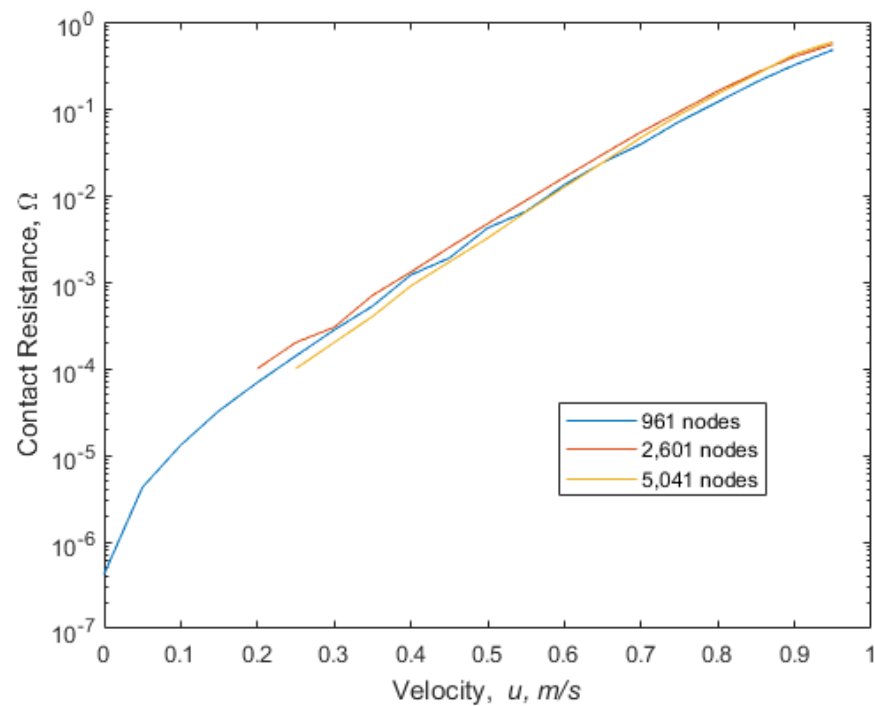


**Figure 3.** Predicted contact resistance as a function of sliding velocity using varying mesh densities.

### 3. Results and Discussion

The numerical scheme can be used to make a variety of predictions about the performance of an electrical contact when liquid lubrication is present. Unless noted otherwise, the hypothetical surface parameters and material properties listed in Table 1 are employed. The properties and forces employed are meant to mimic those seen in some common electrical connectors [57–61]. Even though the applied load appears small, the scale of the contact is small enough that the pressures are high enough to cause significant deformations of the surfaces. Using classic elastic Hertz theory, the approximate maximum contact pressure is 87 MPa and the normal displacement is 0.77 micrometers, which is on the order of the film thickness and roughness. This is often also seen in non-conformal surface contacts such as spheres and cylinders, and in elasto-hydrodynamic contacts as well.

**Table 1.** Geometry and tin material properties.

$R$	0.01 m
Width	0.001 m
$\sigma$	0.5 $\mu\text{m}$
$\eta$	$10^9 \text{ m}^2$
$R_{peak}$	100 $\mu\text{m}$
$E$	41.4 GPa
$S_y$	14 MPa
$\nu$	0.36
$\mu$	0.1 Pa·s
$\rho$	$1.15 \times 10^{-7} \Omega/\text{m}$

The roughness shown is considered to be the combined effective roughness between the surfaces. Note that the solid materials properties ( $E$ ,  $\nu$ , and  $S_y$ ) are for a typical tin

material, which is commonly used in electrical contacts. Both surfaces of the contact are considered to be tin, and that is considered using the effective elastic modulus:

$$\frac{1}{E'} = \frac{(1 - \nu_1^2)}{E_1} + \frac{(1 - \nu_2^2)}{E_2} \quad (19)$$

First, the predicted contact resistance at a contact force of 5N as a function of sliding velocity is shown in Figure 4 for different values of surface roughness. This is a similar representation as the Stribeck curve that is often used to describe friction of different regimes of lubrication. In Figure 4, the contact resistance increases several orders of magnitude as the velocity is increased. As the velocity increases, the fluid pressure increases and pushes the surfaces apart, thus reducing the amount of solid contact between the rough surfaces. It is assumed that the conductivity of the fluid is very small compared to the solid and is effectively nil. Based on this Figure 4, it is clear that the contact resistance could increase significantly when any sliding occurs between the surfaces.

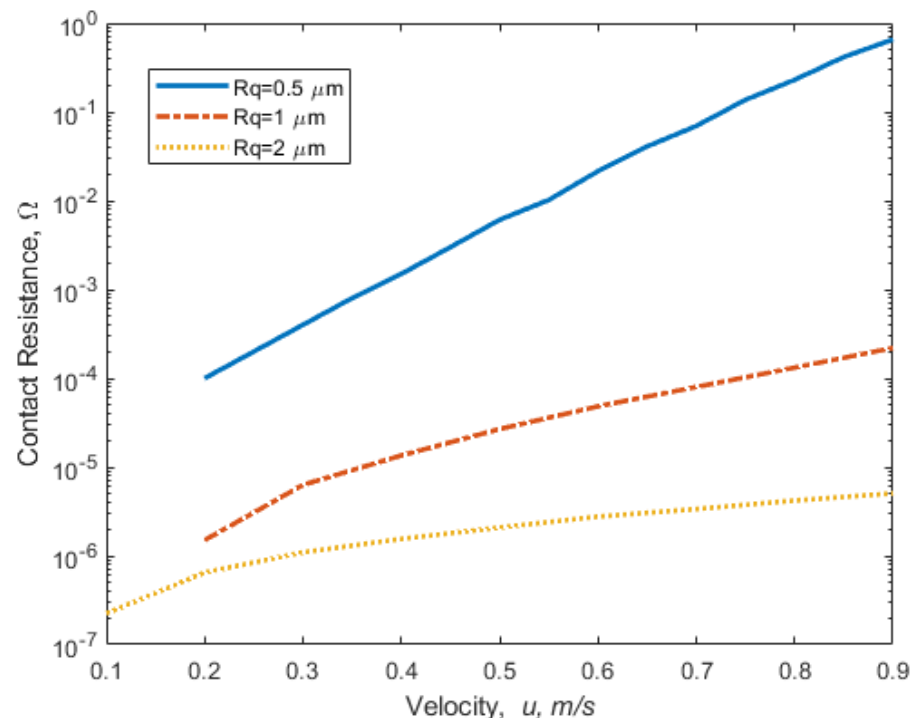


**Figure 4.** Predicted contact resistance as a function of sliding velocity also considering various values of effective surface roughness.

Moreover, in Figure 4, the influence of the effective surface roughness is explored. Note that this is the effective roughness obtained by combining the RMS surface roughness of the two contact surfaces together. It is clear that surface roughness plays an important role in facilitating solid contact between the surfaces. A higher roughness allows for the peaks or asperities to cross the lubricating film at greater thicknesses. As shown in Figure 4, as the surface roughness is increased the contact resistance decreases. Note that in contacts without a lubricant the rough surfaces may actually have a higher contact resistance [62], but due to the effect of the isolating non-conductive film, the roughness plays a positive role here.

To further illustrate the influence of sliding and the liquid lubricant, the predicted coefficient of friction versus sliding velocity is also plotted in Figure 5, using the same code described above. As shown, as the velocity increases the friction first, rapidly lowers and, then, reaches a nearly constant low value. As the sliding speed increases, the lifting pressure generated by the lubricating film also increases and carries more and more of the externally applied force,  $F$ . The almost constant low friction value is when the surfaces are

almost completely separated by a lubricating film. The friction here actually increases a small amount as the thickness of the lubricating film increases. However, when this film separates the surface, it also reduces the real contact area between the surfaces to practically nil, and produces a very high contact resistance.

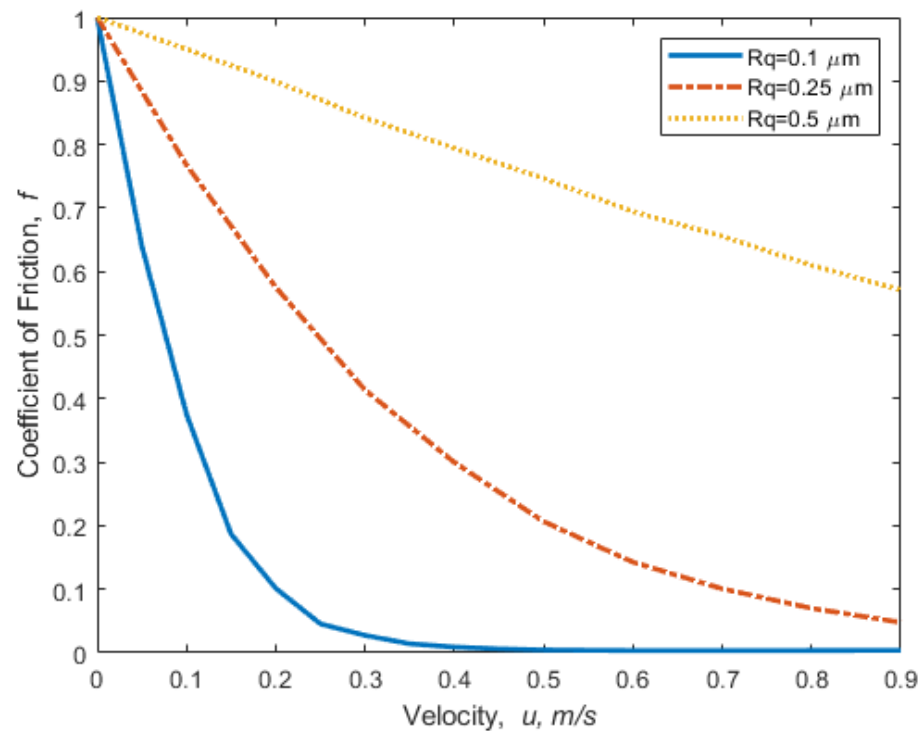


**Figure 5.** Predicted friction coefficient as a function of sliding velocity, i.e., Stribeck curves.

Next, the radius of the cylinder in contact is varied. The results of this could help engineers to select curvatures for electrical connectors that are planned to be lubricated while in service. The predicted contact resistance as a function of sliding speed is shown in Figure 6. As shown, a smaller radius for the contact surface appears to reduce the overall contact resistance. The generated lubricant pressures from sliding depend on the geometry of the surfaces. When the surfaces come closer together in the direction of sliding, it is identified as a converging gap. The converging gap geometry is necessary for the fluid pressure to generate lift. This is in agreement to the elasto-hydrodynamic formulations of Hamrock and Dowson, which predicted that the minimum film thickness decreased with the radius of the geometry. The smaller radius tends to produce less lift than the larger radius. A similar prediction is also shown by the friction in the Stribeck curve shown in Figure 7. The friction increases with smaller radii of the macro-scale surface. These results suggest that connectors for use with lubricants should be designed with surfaces that have a smaller radius of curvature.

The applied force,  $F$ , was also varied and these results are shown in Figure 8. It was found that the normalization used by the popular Stribeck curve (i.e., velocity is divided by the applied force and used on the x-axis) is effective at collapsing the results for this case. The Stribeck curve is shown in Figure 9 to be collapsed, but not perfectly. Note that the Stribeck curve is usually applied to relatively rigid surfaces such as hydrodynamic journal or sliding bearings, whereas in the current case, the macro-scale elastic deformations due to the high pressures is significant (this condition is commonly referred to as elasto-hydrodynamic lubrication).

As shown in Figure 8, this Stribeck normalization successfully collapses the curves onto themselves. Nonetheless, increasing the force does have the effect of reducing the film thickness and keeping the contacts in solid contact. Of course, in a sliding electrical contact, the

increased force could in some cases also increase the wear and surface damage. In other cases, such as when the sliding motion is due to vibrations, the increased force will also increase friction that could anchor the surfaces so that no sliding motion occurs. In general, increasing the normal force improves the resistance of electrical contacts containing lubrication.

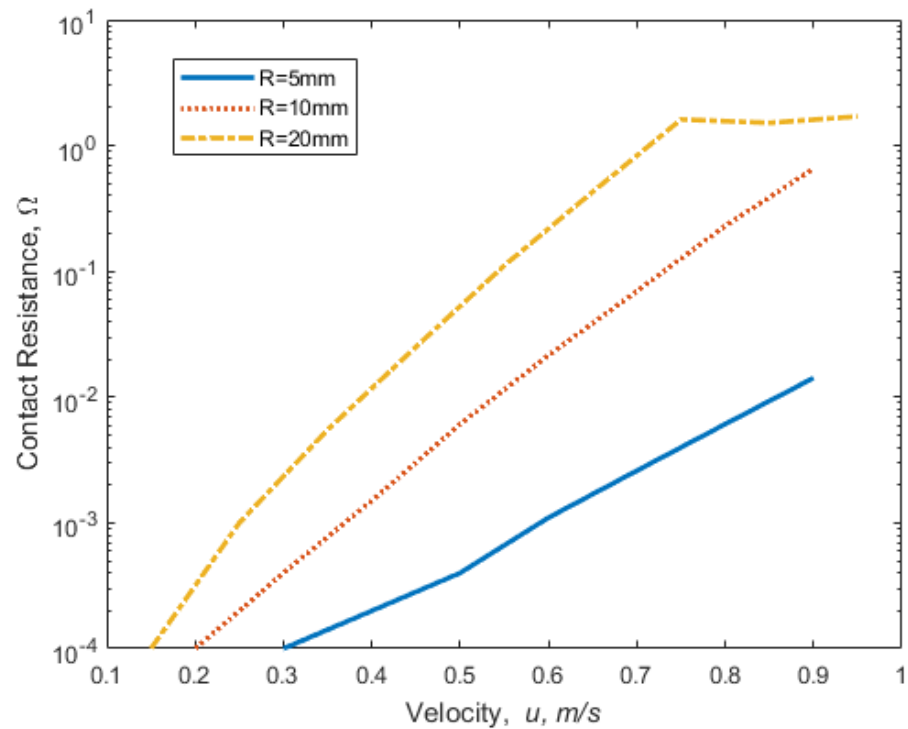


Figure 6. Predicted contact resistance as a function of sliding speed for various macro-scale radii.

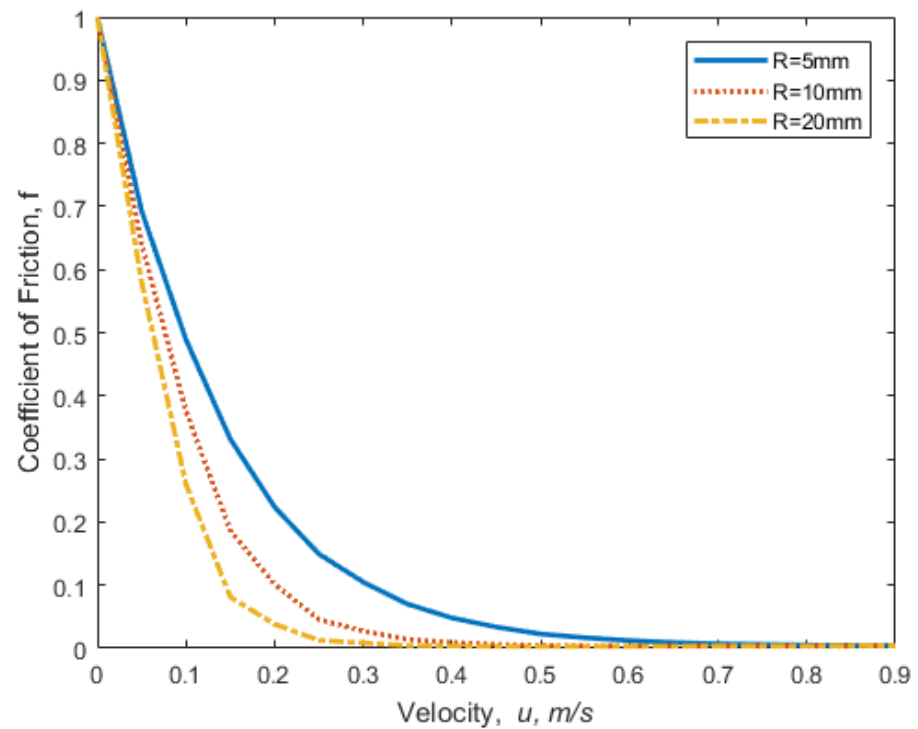


Figure 7. Predicted friction coefficient with various radii.

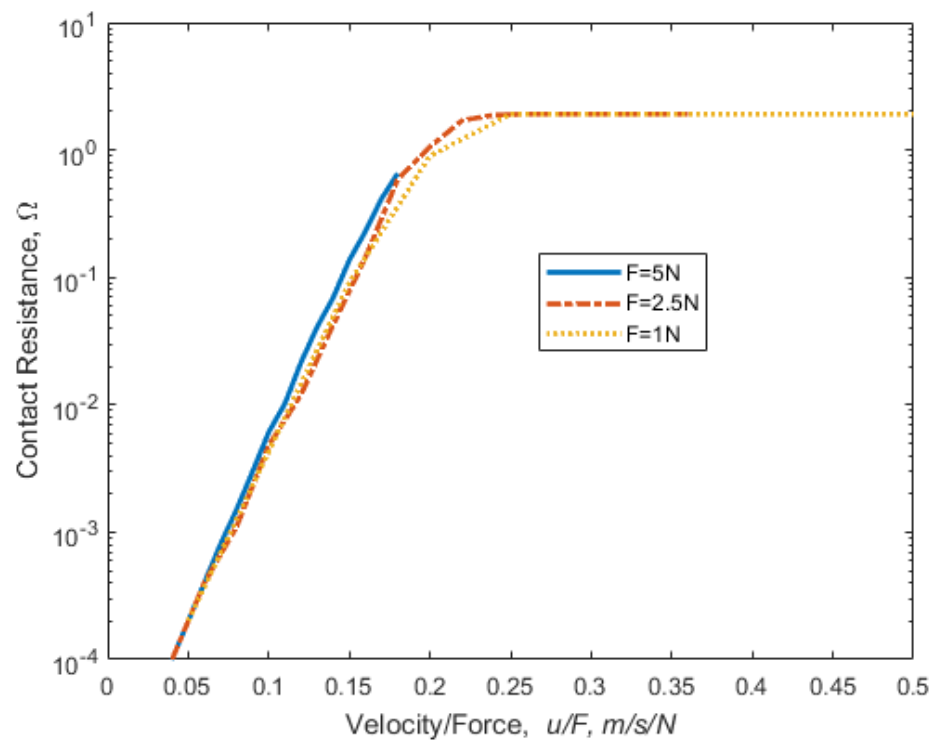


Figure 8. The predicted contact resistance for various loads and speeds.

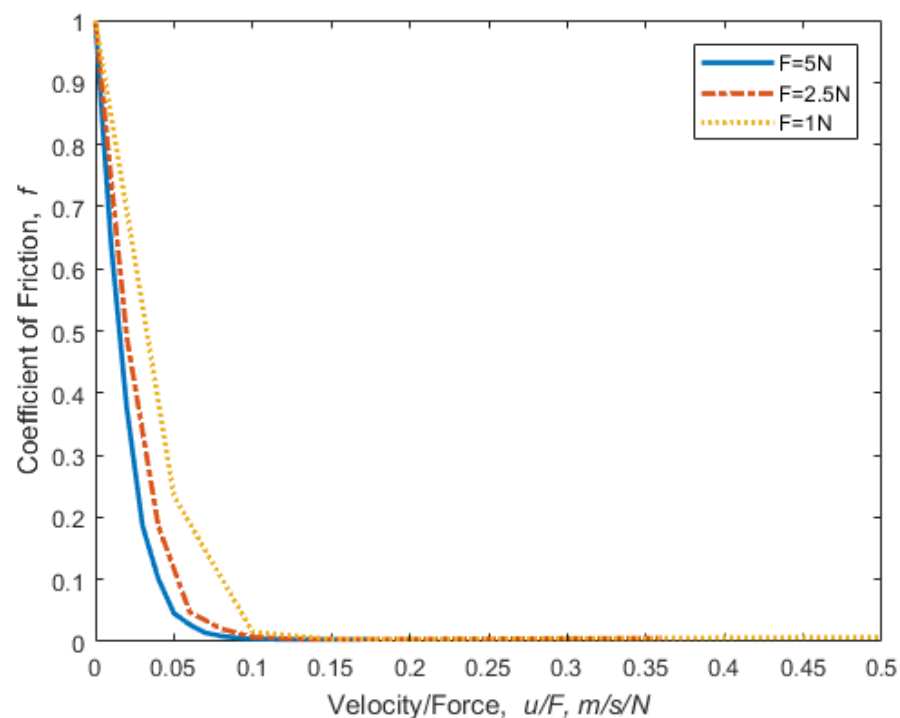


Figure 9. Coefficient of friction predicted for various loads and speed.

Finally, the viscosity of the lubricating fluid between the surfaces is also varied, as shown in Figure 10. The conventional Stribeck curve normalization was also attempted for use here to collapse the results onto one curve, but unlike the variation in force results, the normalization was not effective. Note that in the Stribeck curve the Hersey number is usually used on the x-axis and is the viscosity multiplied by the velocity and divided by the force or average pressure ( $\mu \cdot U/F$ ). Instead, as with the earlier figures, the contact

resistance and friction are just plotted versus the velocity (see Figures 10 and 11). As shown in Figure 10, the reduction of the viscosity helps for the solid surfaces to maintain electrical contact. The lower viscosities reduce the pressure generated by the fluid in sliding and therefore they cannot overcome the externally applied force as easily, which also increases friction.

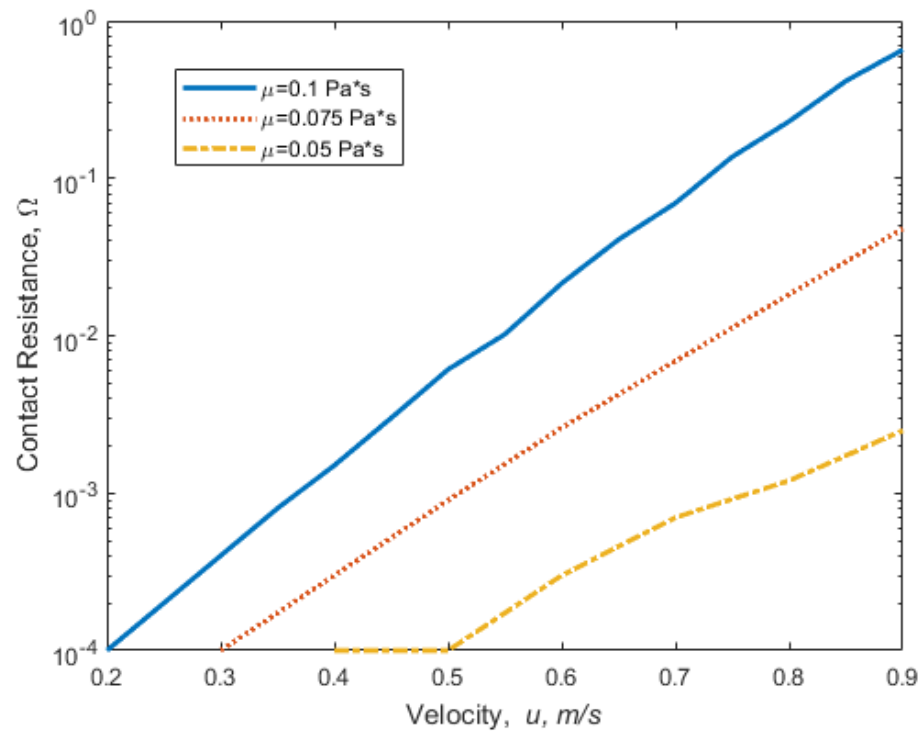


Figure 10. The effect of viscosity on the contact resistance of the lubricated contact.

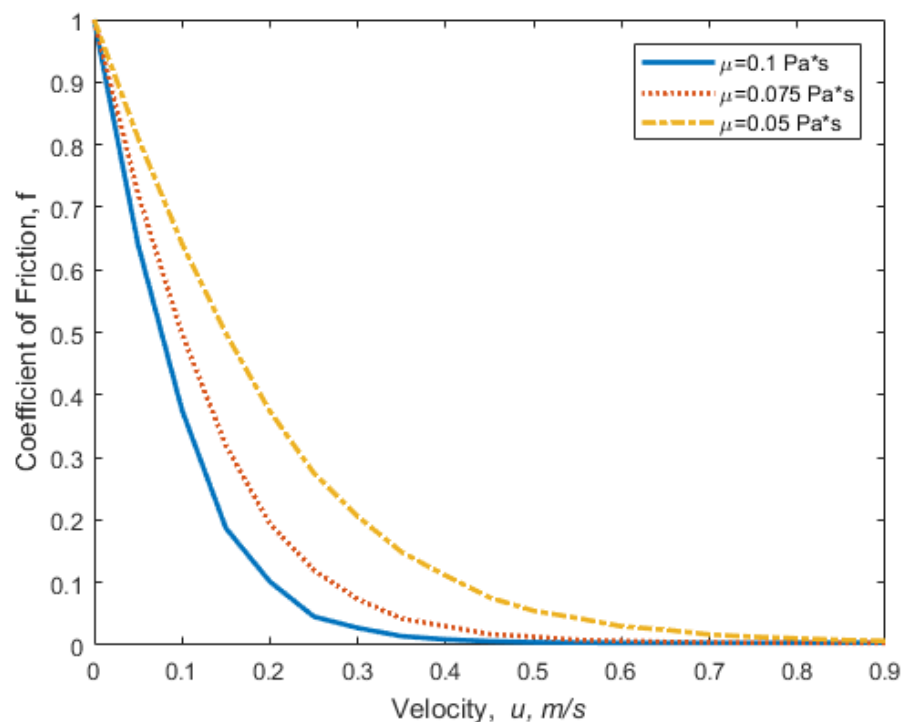


Figure 11. The predicted friction and the influence of different lubricant viscosities.

#### 4. Conclusions

A multiphase numerical model of a sliding rough curved electrical contact that considers both the solid and fluid mechanics is constructed. The model couples the solid and fluid mechanics through the total load carried by the connector, and by the deformation influencing both the fluid and rough surface contact pressures. Roughness is considered through flow factors and a statistical elastic-plastic rough surface contact model.

The model is used to study the qualitative behavior of electrical contacts when parameters such as roughness, macro-scale curvature, applied force, sliding speed and viscosity are varied. These results might be used by engineers to improve the design of lubricated electrical contacts. Rougher surfaces are found to lower the contact resistance by allowing the surfaces to cross the non-conductive lubricant film thickness. Likewise, smaller radii of curvatures for the macro-scale geometry (i.e., the cylinder) also reduces the hydrodynamic lift and reduces electrical contact resistance.

Increasing the force helps to overcome the pressure created by the sliding motion on the lubricating fluid. Therefore, the contact resistance in general improves when higher forces are applied to a lubricated electrical contact. Lowering the viscosity also improves the solid contact between the surfaces, as it reduces the lifting capacity of the fluid.

In the future, we also hope to qualitatively and quantitatively verify the predictions of the model. As noted in some of the cited works, this measurement can be difficult to make. This is because the electrical circuit crosses not only the lubricated contact but also other moving surfaces or bearings in the experimental test rig.

**Author Contributions:** Conceptualization, R.L.J.; methodology, R.L.J.; formal analysis, R.L.J. and S.A.; investigation, S.A. and R.L.J.; writing—original draft preparation, S.A. and R.L.J.; writing—review and editing, S.A. All authors have read and agreed to the published version of the manuscript.

**Funding:** This research received no external funding.

**Conflicts of Interest:** The authors declare no conflict of interest.

#### Nomenclature

$d$	distance between the mean of the surface asperities or peaks
$E$	elastic modulus
$F$	applied force
$f$	friction coefficient
$G$	Gaussian asperity height distribution
$h$	film thickness, separation of mean surface height
$p$	fluid pressure
$P$	contact force
$R_{peak}$	asperity radius of curvature
$S_y$	yield strength
$U$	sliding velocity
$x, y, z$	Cartesian coordinate system
$\delta$	surface deformation
$\eta$	areal asperity density
$\phi$	flow factor for modified Reynolds equation
$\mu$	dynamic fluid viscosity
$\sigma$	RMS roughness
$\nu$	Poisson's ratio

#### References

1. Chudnovsky, B.H. *Lubrication of Electrical and Mechanical Components in Electric Power Equipment*; CRC Press: Boca Raton, FL, USA, 2019.
2. Johnson, K.L. *Contact Mechanics*; Cambridge University Press: Cambridge, UK, 1985.
3. Jackson, R.L. Chapter 14: Lubrication. In *Handbook of Lubrication and Tribology, Volume II: Theory and Design*; Bruce, R.W., Ed.; CRC Press: Boca Raton, FL, USA, 2012; pp. 14.1–14.14.

4. Williams, J.A.; Kennedy, F.E. Engineering Tribology. *J. Tribol.* **1998**, *120*, 644. [[CrossRef](#)]
5. Campbell, W. The lubrication of electrical contacts. *IEEE Trans. Compon. Hybrids Manuf. Technol.* **1978**, *1*, 4–16. [[CrossRef](#)]
6. Chudnovsky, B.H. Lubrication of electrical contacts. In Proceedings of the Fifty-First IEEE Holm Conference on Electrical Contacts, Chicago, IL, USA, 26–28 September 2005; pp. 107–114. [[CrossRef](#)]
7. Sawa, K.; Watanabe, Y.; Ueno, T. Effect of lubricant on sliding conditions in Au-plated slip-ring system for small electric power transfer. In Proceedings of the 2014 IEEE 60th Holm Conference on Electrical Contacts (Holm), New Orleans, LA, USA, 12–15 October 2014; pp. 1–6.
8. Sawa, K.; Takemasa, Y.; Watanabe, Y.; Ueno, T.; Yamanoi, M. Fluctuation components of contact voltage at AgPd brush and Au-plated slip-ring system with lubricant. In Proceedings of the 2015 IEEE 61st Holm Conference on Electrical Contacts (Holm), San Diego, CA, USA, 11–14 October 2015; pp. 250–255.
9. Jackson, R.L.; Coker, A.B.; Tucker, Z.; Hossain, M.S.; Mills, G. An Investigation of Silver-Nanoparticle-Laden Lubricants for Electrical Contacts. *IEEE Trans. Compon. Packag. Manuf. Technol.* **2018**, *9*, 193–200. [[CrossRef](#)]
10. Crilly, L.; Jackson, R.L.; Bond, S.; Mills, G.; Bhargava, S. An Investigation of the Electrical Contact Resistance Change, Lubrication, and Wear Properties of a Nanolubricant. In Proceedings of the 2020 IEEE 66th Holm Conference on Electrical Contacts and Intensive Course (HLM), San Antonio, TX, USA, 30 September–7 October 2020; pp. 1–7.
11. Cao, Z.; Xia, Y.; Liu, L.; Feng, X. Study on the conductive and tribological properties of copper sliding electrical contacts lubricated by ionic liquids. *Tribol. Int.* **2019**, *130*, 27–35. [[CrossRef](#)]
12. Ko, S.-D.; Seo, M.-H.; Yoon, Y.-H.; Han, C.-H.; Lim, K.-S.; Kim, C.-K.; Yoon, J.-B. Investigation of the Nanoparticle Electrical Contact Lubrication in MEMS Switches. *J. Microelectromech. Syst.* **2017**, *26*, 1417–1427. [[CrossRef](#)]
13. Berman, D.; Erdemir, A.; Sumant, A.V. Graphene as a protective coating and superior lubricant for electrical contacts. *Appl. Phys. Lett.* **2014**, *105*, 231907. [[CrossRef](#)]
14. Lang, H.; Xu, Y.; Zhu, P.; Peng, Y.; Zou, K.; Yu, K.; Huang, Y. Superior lubrication and electrical stability of graphene as highly effective solid lubricant at sliding electrical contact interface. *Carbon* **2021**, *183*, 53–61. [[CrossRef](#)]
15. Achanta, S.; Drees, D. Effect of lubrication on fretting wear and durability of gold coated electrical contacts under high frequency vibrations. *Tribol.-Mater. Surf. Interfaces* **2008**, *2*, 57–63. [[CrossRef](#)]
16. Kaushik, L.; Azarian, M.H.; Pecht, M. Fretting Performance Comparison between PFPE and PAO Based Lubricants for Lightly-Loaded Gold-Plated Electrical Contacts. In Proceedings of the 2019 IEEE Holm Conference on Electrical Contacts, Milwaukee, WI, USA, 14–18 September 2019.
17. Chaudhary, R.; Kaushik, L.; Azarian, M.H.; Pecht, M. Comparison between Synthetic Oil Lubricants for Reducing Fretting Degradation in Lightly Loaded Gold-Plated Contacts. 2021. Available online: <https://www.researchsquare.com/article/rs-476954/v1> (accessed on 15 April 2021).
18. Swingler, J. The automotive connector: The influence of powering and lubricating a fretting contact interface. *Proc. Inst. Mech. Eng. Part D J. Automob. Eng.* **2000**, *214*, 615–623. [[CrossRef](#)]
19. Graton, O.; Fouvry, S.; Enquebecq, R.; Petit, L. Effect of Lubrication on DC and RF Electrical Endurance of Gold Plated Contacts Subjected to Fretting Wear. In Proceedings of the 2018 IEEE Holm Conference on Electrical Contacts, Albuquerque, NM, USA, 14–18 October 2018; pp. 426–434.
20. Fu, Y.; Qin, H.; Xu, X.; Zhang, X.; Guo, Z. The effect of surface texture and conductive grease filling on the tribological properties and electrical conductivity of carbon brushes. *Tribol. Int.* **2021**, *153*, 106637. [[CrossRef](#)]
21. Noel, S.; Brezard-Oudot, A.; Chretien, P.; Alamarguy, D. Fretting behaviour of tinned connectors under grease lubrication. In Proceedings of the 2017 IEEE Holm Conference on Electrical Contacts, Denver, CO, USA, 10–13 September 2017; pp. 109–116.
22. Larsson, E.; Andersson, A.M.; Rudolphi, Å.K. Grease lubricated fretting of silver coated copper electrical contacts. *Wear* **2017**, *376–377*, 634–642. [[CrossRef](#)]
23. Amada, Y.; Sawa, K.; Ueno, T. Effects of lubricant oil on sliding contact phenomena in carbon brush-slip ring system. In Proceedings of the 2017 IEEE Holm Conference on Electrical Contacts, Denver, CO, USA, 10–13 September 2017; pp. 182–186.
24. Gohar, R. *Elastohydrodynamics*; World Scientific: Singapore, 2001.
25. Gohar, R.; Cameron, A. Optical Measurement of Oil Film Thickness under Elasto-hydrodynamic Lubrication. *Nature* **1963**, *200*, 458–459. [[CrossRef](#)]
26. Jackson, A.; Cameron, A. An Interferometric Study of the EHL of Rough Surfaces. *ASLE Trans.* **1976**, *19*, 50–60. [[CrossRef](#)]
27. Mehdigoli, H.; Rahnejat, H.; Gohar, R. Vibration response of wavy surfaced disc in elasto-hydrodynamic rolling contact. *Wear* **1990**, *139*, 1–15. [[CrossRef](#)]
28. Teodorescu, M.; Rahnejat, H.; Gohar, R.; Dowson, D. Harmonic decomposition analysis of contact mechanics of bonded layered elastic solids. *Appl. Math. Model.* **2007**, *33*, 467–485. [[CrossRef](#)]
29. Patir, N.; Cheng, H.S. An Average Flow Model for Determining Effects of Three-Dimensional Roughness on Partial Hydrodynamic Lubrication. *J. Lubr. Technol.* **1978**, *100*, 12–17. [[CrossRef](#)]
30. Patir, N.; Cheng, H.S. Application of Average Flow Model to Lubrication Between Rough Sliding Surfaces. *ASME J. Tribol.* **1979**, *101*, 220–230. [[CrossRef](#)]
31. Dmochowski, W.M.; Dadouche, A.; Fillon, M. Finite Difference Method for Fluid-Film Bearings. In *Encyclopedia of Tribology*; Springer Science and Business Media LLC: Berlin, Germany, 2013; pp. 1137–1143.
32. Szeri, A.Z. *Fluid Film Lubrication*; Cambridge University Press: Cambridge, UK, 2010.

33. Booser, E.R. *CRC Handbook of Lubrication. Theory and Practice of Tribology. Volume II: Theory and Design*; CRC Press: Boca Raton, FL, USA, 1984.
34. Zhao, B.; Dai, X.-D.; Zhang, Z.-N.; Xie, Y.-B. A new numerical method for piston dynamics and lubrication analysis. *Tribol. Int.* **2016**, *94*, 395–408. [[CrossRef](#)]
35. Zhang, X.; Xu, Y.; Jackson, R.L. A mixed lubrication analysis of a thrust bearing with fractal rough surfaces. *Proc. Inst. Mech. Eng. Part J J. Eng. Tribol.* **2020**, *234*, 608–621. [[CrossRef](#)]
36. Zhang, X.; Jackson, R.L. A mixed lubrication analysis of a flat-land thrust bearing with a surface optimisation method. *Lubr. Sci.* **2021**, *33*, 335–346. [[CrossRef](#)]
37. Jackson, R.L.; Green, I. The Behavior of Thrust Washer Bearings Considering Mixed Lubrication and Asperity Contact. *Tribol. Trans.* **2006**, *49*, 233–247. [[CrossRef](#)]
38. Jackson, R.L.; Green, I. The Thermoelastic Behavior of Thrust Washer Bearings Considering Mixed Lubrication, Asperity Contact, and Thermoviscous Effects. *Tribol. Trans.* **2008**, *51*, 19–32. [[CrossRef](#)]
39. Angadi, S.; Jackson, R.L.; Choe, S.-Y.; Flowers, G.T.; Lee, B.-Y.; Zhong, L. A Multiphysics Finite Element Model of a 35A Automotive Connector Including Multiscale Rough Surface Contact. *J. Electron. Packag.* **2012**, *134*, 011001. [[CrossRef](#)]
40. Angadi, S.V.; Jackson, R.L.; Pujar, V.; Tushar, M.R. A Comprehensive Review of the Finite Element Modeling of Electrical Connectors Including Their Contacts. *IEEE Trans. Compon. Packag. Manuf. Technol.* **2020**, *10*, 836–844. [[CrossRef](#)]
41. Polchow, J.R.; Angadi, S.; Jackson, R.; Choe, S.-Y.; Flowers, G.T.; Lee, B.-Y.; Zhong, L. A Multi-Physics Finite Element Analysis of Round Pin High Power Connectors. In Proceedings of the 2010 Proceedings of the 56th IEEE Holm Conference on Electrical Contacts, Charleston, SC, USA, 4–7 October 2010; pp. 1–9.
42. Kogut, L.; Etsion, I. Electrical Conductivity and Friction Force Estimation in Compliant Electrical Connectors. *Tribol. Trans.* **2000**, *43*, 816–822. [[CrossRef](#)]
43. Leidner, M.; Schmidt, H.; Myers, M.; Schlaak, H.F. A new simulation approach to characterizing the mechanical and electrical qualities of a connector contact. *Eur. Phys. J. Appl. Phys.* **2010**, *49*, 22909. [[CrossRef](#)]
44. Liu, H.; Leray, D.; Colin, S.; Pons, P.; Broué, A. Finite Element Based Surface Roughness Study for Ohmic Contact of Microswitches. In Proceedings of the 2012 IEEE 58th Holm Conference on Electrical Contacts (Holm), Portland, OR, USA, 23–26 September 2012; pp. 1–10.
45. Israel, T.; Gatzsche, M.; Schlegel, S.; Grosmann, S.; Kufner, T.; Freudiger, G. The impact of short circuits on contact elements in high power applications. In Proceedings of the 2017 IEEE Holm Conference on Electrical Contacts, Denver, CO, USA, 10–13 September 2017; pp. 40–49.
46. Jackson, R.L.; Green, I. A Statistical Model of Elasto-plastic Asperity Contact between Rough Surfaces. *Tribol. Int.* **2006**, *39*, 906–914. [[CrossRef](#)]
47. An, B.; Wang, X.; Xu, Y.; Jackson, R.L. Deterministic elastic-plastic modelling of rough surface contact including spectral interpolation and comparison to theoretical models. *Tribol. Int.* **2019**, *135*, 246–258. [[CrossRef](#)]
48. Jackson, R.L.; Green, I.; Marghitu, D.B. Predicting the coefficient of restitution of impacting elastic-perfectly plastic spheres. *Nonlinear Dyn.* **2010**, *60*, 217–229. [[CrossRef](#)]
49. Greenwood, J.A.; Williamson, J.B.P. Contact of nominally flat surfaces. *Proc. R. Soc. Lond. Ser. A Math. Phys. Sci.* **1966**, *295*, 300–319. [[CrossRef](#)]
50. Front, I. *The Effects of Closing Force and Surface Roughness on Leakage in Radial Face Seals*; Technion, Israel Institute of Technology: Haifa, Israel, 1990.
51. McCool, J.I. Relating Profile Instrument Measurements to the Functional Performance of Rough Surfaces. *J. Tribol.* **1987**, *109*, 264–270. [[CrossRef](#)]
52. Etsion, I.; Kligerman, Y.; Kadin, Y. Unloading of an elastic–plastic loaded spherical contact. *Int. J. Solids Struct.* **2005**, *42*, 3716–3729. [[CrossRef](#)]
53. Jackson, R.L.; Chusoipin, I.; Green, I. A Finite Element Study of the Residual Stress and Strain Formation in Spherical Contacts. *ASME J. Tribol.* **2005**, *127*, 484–493. [[CrossRef](#)]
54. Yang, H.; Green, I. Analysis of displacement-controlled fretting between a hemisphere and a flat block in elasto-plastic contacts. *J. Tribol.* **2019**, *141*, 031401. [[CrossRef](#)]
55. Holm, R. *Electric Contacts*; Springer: New York, NY, USA, 1967.
56. Cooper, M.G.; Mikic, B.B.; Yovanovich, M.M. Thermal contact conductance. *Int. J. Heat Mass Transf.* **1969**, *12*, 279–300. [[CrossRef](#)]
57. Siddaiah, A.; Kasar, A.K.; Khosla, V.; Menezes, P.L. In-Situ Fretting Wear Analysis of Electrical Connectors for Real System Applications. *J. Manuf. Mater. Process.* **2019**, *3*, 47. [[CrossRef](#)]
58. Sharma, A.; Ahn, B. Dry Sliding Wear Behavior of Sn and NiSn Overlays on Cu Connectors. *Tribol. Lett.* **2018**, *66*, 136. [[CrossRef](#)]
59. Song, J.; Yuan, H.; Schinow, V. Fretting corrosion behavior of electrical contacts with tin coating in atmosphere and vacuum. *Wear* **2019**, *426–427*, 1439–1445. [[CrossRef](#)]
60. Jackson, R.; Ashurst, W.R.; Flowers, G.T.; Angadi, S.; Choe, S.-Y.; Bozack, M.J. The Effect of Initial Connector Insertions on Electrical Contact Resistance. In Proceedings of the Electrical Contacts-2007 Proceedings of the 53rd IEEE Holm Conference on Electrical Contacts, Pittsburgh, PA, USA, 16–19 September 2007; pp. 17–24.

61. Angadi, S.; Wilson, W.E.; Jackson, R.L.; Flowers, G.T.; Rickett, B.I. A Multi-Physics Finite Element Model of an Electrical Connector Considering Rough Surface Contact. In Proceedings of the 2008 Proceedings of the 54th IEEE Holm Conference on Electrical Contacts, Orlando, FL, USA, 27–29 October 2008; pp. 168–177.
62. Zhang, X.; Jackson, R.L. The influence of multiscale roughness on the real contact area and contact resistance between real reference surfaces. In Proceedings of the ICEC 2014—The 27th International Conference on Electrical Contacts, Dresden, Germany, 22–26 June 2014; VDE: Berlin, Germany.